JOURNAL
OF THE AMERICAN CHEMICAL SOCIETY

VOLUME 101, NUMBER 11 MAY 23, 1979

Vibronic Coupling Model for Mixed-Valence Compounds. Comparisons and Predictions

K. Y. Wong,[1a] P. N. Schatz,*[1a] and S. B. Piepho[1b]

Contribution from the Departments of Chemistry, University of Virginia, Charlottesville, Virginia 22901, and Randolph-Macon Woman's College, Lynchburg, Virginia 24503. *Received November 9, 1978*

Abstract: Some important features of a vibronic coupling model for mixed valence systems (PKS model) are examined in detail and compared with the predictions of earlier, more approximate treatments. Applying the semiclassical Franck-Condon principle to the PKS equations, analytical formulas are derived for the first three absorption moments of the intervalence band in localized systems. In the localized (strong vibronic coupling) limit, these reduce to earlier formulas which have been widely used in the literature. Through detailed comparisons with exact solutions of the PKS model over a wide range of parameters, one obtains a clear picture of the limited range of validity of such formulas as a function of vibronic and electronic coupling and the temperature. It is suggested that the parameters of the PKS model can be extracted through quantitative examination of intervalence band contours and will give much significant information about mixed-valence systems. Using a static model, an expression is derived for the "degree of delocalization" of mixed-valence systems which reduces in the localized limit to a formula which has been widely used. An alternative definition based on the PKS model is developed which has much more general validity. The Robin and Day classification scheme for mixed-valence systems is reformulated using the PKS parameters. Finally, a table is presented which summarizes the range of validity of the various formulas discussed in the paper.

I. Introduction

A typical mixed-valence system contains ions in two different oxidation states. Its electronic spectrum characteristically displays a low-energy band (the intervalence band) which cannot be attributed to either ion alone, since it results from transitions within a ground vibronic manifold arising from coupling of the constituent ions. About 10 years ago, Robin and Day[2] surveyed these systems and proposed a classification scheme which has stimulated much interest in mixed-valence compounds, a rich variety of them having been studied over a long period of time.[2,3] Considerable theoretical work has appeared,[2,4-6] and formulas have been presented which relate the intervalence bandwidth, transition energy, and "degree of delocalization" of the system to various experimental observables.

There is much current interest in intervalence transitions since they can give detailed information about the potential surfaces arising from the coupling of the ions and thus can relate optical and thermal electron transfer processes.[3] These ideas have also been applied to biomolecules,[5a] and the existence of an intervalence band, assigned to an electron transfer transition in the bound model system cytochrome c-$Fe(CN)_6$, has been experimentally demonstrated.[5b]

Recently, Piepho, Krausz, and Schatz[7] (PKS) outlined a vibronic coupling model which, for the first time, permits an actual calculation of the intervalence absorption profile as a function of temperature. Since the PKS treatment provides explicit eigenvalues and eigenfunctions for the complete ground vibronic manifold, it is also possible to make well-defined statements about valence trapping and various experimental observables.

In this paper we examine various predictions of the PKS model and relate these to previous work. The restricted range of validity of previous formulas[4-6] becomes clearly apparent.

II. The PKS Model

The PKS model has been discussed in detail elsewhere;[7,8] we summarize here certain essential features, some of which may not be immediately apparent from the more formal treatment given previously.[7] Let us first suppose that a mixed-valence system consists of two octahedral "monomer" units, A and B, whose nuclei go into each other under a symmetry operation. This is the symmetrical case, A = B. The Creutz and Taube complex (**1**) is an example except that the

1

monomer symmetry is only approximately O_h. It is found[7] that *two* interaction parameters are essential for a meaningful discussion of those properties which give mixed-valence systems their rather unique characteristics. One (denoted by ϵ) is a measure of the interaction between the two monomer centers and is treated as a purely electronic coupling. The other (denoted by λ) is a measure of vibronic coupling and is directly proportional to the *difference* in the equilibrium value of the a_{1g} monomer normal coordinate in the two different oxidation states which characterize the mixed-valence compound.

If the PKS model is solved in the *static* limit (zero nuclear kinetic energy), the results are[7]

0002-7863/79/1501-2793$01.00/0

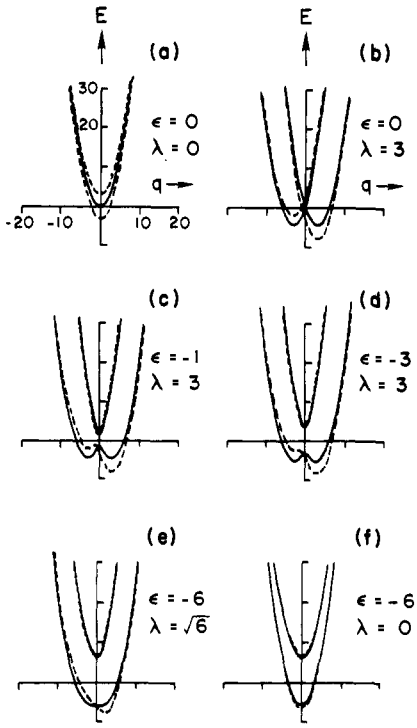

Figure 1. Potential energy surfaces (in units of $h\nu_-$) in q space according to eq 1 for a range of values of the parameters ϵ and λ. The solid curves apply for $W = 0$, the symmetrical (A = B) case, and the dashed curves apply for $W = 3$.

$$\frac{E_1}{h\nu_-} = (q^2/2) - \kappa, \frac{E_2}{h\nu_-} = (q^2/2) + \kappa$$

$$\psi_1 = -\frac{1}{N}[(\epsilon - \kappa)\psi_+ + \sigma\psi_-] \qquad (1)$$

$$\psi_2 = \frac{1}{N}[\sigma\psi_+ - (\epsilon - \kappa)\psi_-]$$

where $N = N(q) \equiv [\sigma^2 + (\epsilon - \kappa)^2]^{1/2}$

$$\kappa = \kappa(q) \equiv [\epsilon^2 + \sigma^2]^{1/2}$$

$$\sigma = \sigma(q) \equiv (\lambda q + W)$$

and $W = 0$ in the symmetrical case. E_1 and E_2 are the potential energies of the lower and upper surfaces in q_- ($\equiv q$) space,[9] and ν_- is the fundamental vibrational frequency associated with this coordinate. ψ_1 and ψ_2 are the *electronic* wave functions corresponding to E_1 and E_2. $\psi_\pm$ are defined by

$$\psi_\pm = \frac{1}{\sqrt{2}}(\psi_a \pm \psi_b) \qquad (2)$$

with $\psi_a \equiv \psi_M{}^A \psi_N{}^B$ and $\psi_b \equiv \psi_N{}^A \psi_M{}^B$, N and M designating oxidation states.

Let us first suppose that ϵ and λ are both zero. Then the potential surface in q_- ($\equiv q$) space[9] consists of two parabolas (in the harmonic approximation) in complete coincidence (solid curve, Figure 1a). If we allow the equilibrium value of Q_A (and Q_B)[9] to be different in the two oxidation states ($\lambda \neq 0$) but maintain zero electronic coupling between the monomer units ($\epsilon = 0$), the two surfaces separate horizontally (solid curves, Figure 1b). If electronic coupling is now permitted ($\epsilon \neq 0$), two distinct surfaces result whose separation increases as $|\epsilon|$ increases (solid curves, Figures 1c,d). Finally, when vibronic coupling is turned down, the upper surface spreads and the lower surface contracts with the disappearance of the double minimum on the latter at $\lambda^2 = |\epsilon|$ (solid curves, Figure 1e), and when $\lambda = 0$ the two surfaces become identical parabolas, vertically displaced by an energy $|2\epsilon|$ (solid curves, Figure 1f). Qualitatively, Figures 1c,d and 1e,f illustrate respectively the so-called localized (or valence-trapped) and delocalized (or untrapped) cases. In the localized case, there are two most probable configurations in q space which can be depicted as i and ii. In the delocalized case, there is a single

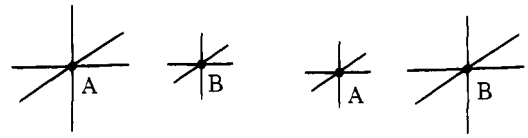

i ii

most probable configuration, iii. Using the Creutz and Taube

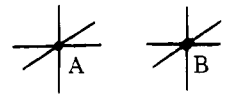

iii

complex as an example, the former is sometimes referred to as the 2-3 ↔ 3-2 and the latter as the $2^1/_2 \leftrightarrow 2^1/_2$ case. In the former there are distinct Ru(II) and Ru(III) species present, whereas in the latter both Ru atom environments are identical. The quantitative expression of these ideas is displayed by a plot of the probability distribution function in q space; such plots are easily made using the PKS model. (See Figure 4, ref 7.) Qualitatively, a system is strongly trapped (localized) if $\lambda^2 \gg |\epsilon|$ and is completely untrapped (delocalized) if $\lambda^2 < |\epsilon|$

The intervalence band arises from transitions between the two potential surfaces. Far-infrared tunneling transitions should also arise from transitions within the lower potential surface.[8] To discuss the spectroscopy of the intervalence band in a quantitative way, one might proceed by writing down vibronic functions on each potential surface and computing population-weighted transition probabilities between the two surfaces. Thus, for example, one could write

$$\Phi_{1,m'} = \psi_1 \chi_{m'}$$
$$\Phi_{2,m} = \psi_2 \chi_m \qquad (3)$$

where ψ_1 and ψ_2 (eq 1) are electronic functions, respectively, on the lower and upper surfaces, and χ_m and $\chi_{m'}$ are corresponding vibrational functions on the two surfaces. If either ϵ or λ is zero, ψ_1 and ψ_2 are seen to be independent of q (even if $W \neq 0$), E_1 and E_2 are harmonic, and χ_m and $\chi_{m'}$ will be harmonic oscillator functions. A conventional discussion in terms of Franck-Condon overlap factors is appropriate.

However, if λ and ϵ are *both* nonzero (Figures 1c-e—the chemically interesting cases!), ψ_1 and ψ_2 are seen to be strong functions of q. Consequently, ψ_1 and ψ_2 do *not* commute with the kinetic energy operator, and one has a pseudo-Jahn-Teller problem;[10] one must take account of the fact that the nuclear motion cannot be confined to a single potential surface (the dynamic problem). *The quantum-mechanical consequence is that simple Born-Oppenheimer vibronic functions (such as eq 3) are inappropriate.* The solutions in general are linear combinations of vibronic functions from both surfaces. Furthermore, ψ_1 and ψ_2 are inconvenient electronic basis functions since they neither commute with the kinetic energy operator nor permit the Franck-Condon approximation to be used.

One finds[7,11] that an appropriate electronic basis is $\psi_\pm$ (eq 2), and it turns out to be extremely convenient to use the complete set of harmonic oscillator functions, $\chi_n(q)$, as the vibrational basis.[11] Solutions are then of the form[7]

$$\Phi^+_\nu = \sum_{\substack{n=0,2\\4}}^{\infty} r_{\nu n}\psi_+\chi_n + \sum_{\substack{n=1,3\\5}}^{\infty} r_{\nu n}\psi_-\chi_n$$

$$\Phi^-_\nu = \sum_{\substack{n=1,3\\5}}^{\infty} s_{\nu n}\psi_+\chi_n + \sum_{\substack{n=0,2,\\4}}^{\infty} s_{\nu n}\psi_-\chi_n \qquad (4)$$

The functions are divided into those which do (− superscript) and those which do not (+ superscript) change sign under interchange of A and B. The $r_{\nu n}$ satisfy the secular equations

$$\sum_{n=0}^{\infty} r_{\nu n}\,(H_{mn} - \delta_{mn} E^{+}_{\nu}) = 0; \quad \begin{matrix} m = 0,1,2\ldots \\ \nu = 0,1,2\ldots \end{matrix} \tag{5}$$

with

$$H_{mn} = \lambda\left[\sqrt{\frac{m}{2}}\,\delta_{m,n+1} + \sqrt{\frac{m+1}{2}}\,\delta_{m,n-1}\right] + \left(m + \frac{1}{2} + (-1)^m\epsilon\right)\delta_{m,n}$$

and exactly analogous equations apply for $s_{\nu n}$ substituting $(-\epsilon)$ for ϵ and E^{-}_{ν} for E^{+}_{ν}. The eigenvalues ($E^{\pm}_{\nu}$) are roots of the corresponding secular determinants.

The dipole strength (intensity) of a vibronic line, $\Phi^{+}_{\nu'} \rightarrow \Phi^{-}_{\nu}$, is given by[7]

$$D(\nu' \rightarrow \nu) = \frac{(N_{\nu'} - N_{\nu})}{N}\,\mathcal{S}^2_{\nu'\nu}\,|\langle\psi_+|m_z|\psi_-\rangle|^2 \tag{6}$$

where $N_{\nu} = \exp(-E_{\nu}/kT)$

$$N = \sum_{\nu} N_{\nu}$$

$$\mathcal{S}_{\nu'\nu} = \sum_{n} r_{\nu' n}\, s_{\nu n} \tag{7}$$

The intervalence band is the totality of lines, $\nu' \rightarrow \nu$, arising from transitions between the two surfaces, and the effect of temperature is expressed through the population factors, N_{ν}.

In the case of an unsymmetrical mixed valence system (A ≠ B), the PKS model requires one additional parameter, W, which is a measure of the difference in zero-point potential energy of the two "monomers".[7] The interchange symmetry is lost and eq 4 is replaced by

$$\Phi_{\nu} = \sum_{n=0}^{\infty} (r_{\nu n}\,\psi_+\,\chi_n + r'_{\nu n}\,\psi_-\,\chi_n) \tag{8}$$

The secular equations are

$$\sum_{n=0}^{\infty} r_{\nu n}\,(H_{mn} - \delta_{mn} E_{\nu}) + \sum_{n=0}^{\infty} r'_{\nu n} H''_{mn} = 0$$

$$\sum_{n=0}^{\infty} r'_{\nu n}\,(H'_{mn} - \delta_{mn} E_{\nu}) + \sum_{n=0}^{\infty} r_{\nu n} H''_{mn} = 0$$

$$H_{mn} = \left(m + \frac{1}{2} + \epsilon\right)\delta_{mn};\; H'_{mn} = \left(m + \frac{1}{2} - \epsilon\right)\delta_{mn}$$

$$H''_{mn} = \lambda\left[\sqrt{\frac{m}{2}}\,\delta_{m,n+1} + \sqrt{\frac{m+1}{2}}\,\delta_{m,n-1}\right] + W\,\delta_{mn} \tag{9}$$

$$m = 0,1,2\ldots \qquad \nu = 0,1,2\ldots$$

It is now necessary to diagonalize a single block twice the size of the two separate blocks obtained in the symmetrical case, and the tridiagonal form (of the symmetrical case) is lost.[7] For transition from a state $\Phi_{\nu'}$ (eq 8 with $\nu = \nu'$), to a state Φ_{ν} (eq 8 with $r_{\nu n}$, $r'_{\nu n}$ replaced respectively by $s_{\nu n}$, $s'_{\nu n}$), eq 6 continues to apply, but eq 7 is replaced by

$$\mathcal{S}_{\nu'\nu} = \sum_{n=0}^{\infty} (r_{\nu' n}\, s'_{\nu n} + r'_{\nu' n}\, s_{\nu n}) \tag{10}$$

Potential surfaces for the case $W = 3$ are shown by the dashed curves in Figure 1. Increasing W always increases localization. We shall find (section III) in the localized limit that λ and W occur together in the form $(\lambda^2 + W)$. Band contours for some representative cases both for $W = 0$ and $W \neq 0$ have been given previously.[7]

III. Semiclassical Treatment of the Localized Case ($\lambda^2 + W \gg |\epsilon|$). Derivation of Earlier Formulas

Though the equations in the PKS model (eq 5 and 9) cannot in general be solved in closed form, in spectroscopic applications the basis can be drastically truncated without significant loss of accuracy. Thus it is possible to produce "exact" solutions for any specified values of the parameters ϵ, λ, and W through computer diagonalizations. It is, however, also possible and quite illuminating to obtain analytical solutions in the semiclassical limit. This leads to several formulas widely quoted in the literature, and subsequent comparisons with the PKS model give a good feel for the probable range of validity of such formulas.

The semiclassical treatment of the Franck-Condon principle was discussed many years ago by Lax.[12] He showed that such a treatment becomes more accurate as both the temperature and electron-phonon coupling (our λ) increase. More recently, Toyozawa and Inoue[13] successfully used this method to discuss Jahn-Teller band shapes.

Let us first consider the symmetrical case (A = B) so that $W = 0$. Elementary considerations (eq 1) show that the height of the barrier on the lower potential surface is given by

$$E_a/h\nu_- = \frac{1}{2}\lambda^2 - |\epsilon| + \epsilon^2/2\lambda^2;\; |\epsilon| \leq \lambda^2 \tag{11}$$

E_a is sometimes referred to as the activation energy for thermal electron transfer. Strong vibronic coupling ($\lambda^2 \gg |\epsilon|$) clearly corresponds to the localized case (Figure 1c) to which we now apply the semiclassical treatment. The band shape function is given by[12,13]

$$F(E) = \frac{\int_{-\infty}^{+\infty} dq e^{-E_1/kT}\,|\langle\psi_1|m_z|\psi_2\rangle|^2\,\delta(E - (E_2 - E_1))}{\int_{-\infty}^{+\infty} dq e^{-E_1/kT}} \tag{12}$$

where the intervalence transition is z polarized[7] if the z axis is chosen to connect the two monomer centers. Here we are using the "high-temperature form" which assumes a Boltzmann population distribution among a continuum of energy levels on the lower potential surface.[13] (Thus the treatment is strictly valid only if $E_a \gg kT \gg h\nu_-$.) Both $|\langle\psi_1|m_z|\psi_2\rangle|^2$ and $(E_2 - E_1)$ will be a function of q. Using E_1, E_2, ψ_1, and ψ_2 from eq 1 and the relation[14]

$$\delta[h\nu - (2h\nu_-)(\epsilon^2 + \lambda^2 q^2)^{1/2}] = \left[\frac{\epsilon^2 + \lambda^2 q^2}{\lambda^2 h\nu_-}\right]^{1/2}\delta\left[q^2 - \left(\frac{\nu^2}{4\nu_-^2} - \epsilon^2\right)\Big/\lambda^2\right] \tag{13}$$

the numerator of eq 12 may be evaluated exactly. The denominator cannot be evaluated analytically, but in the limit, $\lambda^2 \gg |\epsilon|$, has the value $(2\pi kT/h\nu_-)^{1/2}\exp(h\nu_-\lambda^2/2kT)$. Letting $M^2 \equiv |\langle\psi_+|m_z|\psi_-\rangle|^2$, the final result is

$$F(E) = C(\epsilon, \lambda, T, \nu)\,M^2 \times \exp\left\{-\left(\frac{h\nu_-}{2kT\lambda^2}\right)\left(\frac{\nu}{2\nu_-} - \lambda^2\right)^2\right\} \tag{14a}$$

where

$$C(\epsilon, \lambda, T, \nu) \equiv \frac{\epsilon^2}{\lambda h\nu}\left(\frac{h\nu_-}{2\pi kT}\right)^{1/2}\left[\left(\frac{\nu}{2\nu_-}\right)^2 - \epsilon^2\right]^{-1/2}\exp\left(\frac{h\nu_-\epsilon^2}{2kT\lambda^2}\right) \tag{14b}$$

and

$$\nu_{max} \approx \nu_-\,\lambda^2\left[1 + \left(1 - \frac{8kT}{h\nu_-\lambda^2}\right)^{1/2}\right] \tag{14c}$$

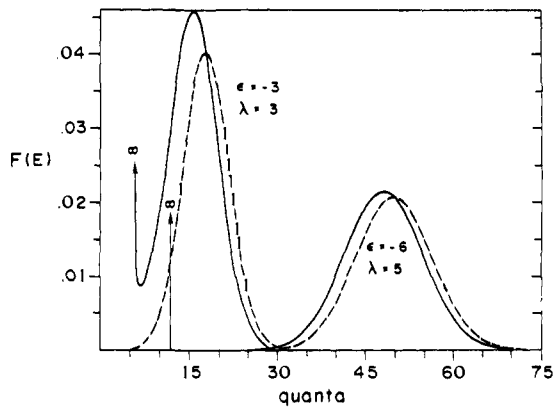

Figure 2. The solid curves are plots of the intervalence band contour $F(E)$ (eq 14) in units of M^2 vs. frequency (in units of ν_- quanta) for $(h\nu_-/2kT) = 1.20$ and $W = 0$. The vertical arrows show the van Hove singularities. The dashed curves are the same except that ν in eq 14b has been replaced by $2\lambda^2\nu_-$.

ν_{max} is obtained by setting $\partial F(E)/\partial E = 0$ and assuming that terms of order ϵ^2/λ^4 are negligible. The full width at half height ($\Delta\nu_{1/2}$) may be approximated by noting that C is a weak function of frequency in the region of strong absorption. If this frequency dependence is ignored, $F(E)$ is a Gaussian for which

$$\Delta\nu_{1/2} \approx 4\nu_- \lambda\sqrt{2 \ln 2}\left(\frac{kT}{h\nu_-}\right)^{1/2} \quad (15)$$

Plots of $F(E)$, eq 14, for two cases are shown in Figure 2. The singularity at $2|\epsilon|\nu_-$ ("van Hove singularity") is a consequence of the one-dimensional nature of the problem and is inherent.[13,15]

In the limit $h\nu_-\lambda^2 \gg kT$, eq 14c becomes $\nu_{max} = 2\nu_-\lambda^2$. This frequency corresponds exactly to the vertical excitation energy (sometimes referred to as E_{op}) from either minimum in the lower potential surface to the upper potential surface, a fact which follows immediately from eq 1. Thus using eq 11

$$E_{op}/E_a = 2\lambda^2 \Big/ \left(\frac{1}{2}\lambda^2 - |\epsilon| + \epsilon^2/2\lambda^2\right) \quad (16a)$$

$$\lim_{(\lambda^2/|\epsilon|) \to \infty} (E_{op}/E_a) = 4 \quad (16b)$$

Equation 16b, which obviously applies only in the localized limit, is quoted in many discussions. Combining eq 14 and 15

$$(h\Delta\nu_{1/2})^2/h\nu_{max} = \frac{32kT \ln 2}{\left[1 + \left(1 - \frac{8kT}{h\nu_-\lambda^2}\right)^{1/2}\right]} \quad (17)$$

and in the limit $h\nu_-\lambda^2 \gg kT$

$$(h\Delta\nu_{1/2})^2/h\nu_{max} = 16kT \ln 2 = 2312 \text{ cm}^{-1} \text{ (at 300 K)} \quad (18)$$

Equation 18 was derived previously[4] and is widely used.

Using the same methods, the unsymmetrical case ($A \neq B$) may be treated, and the results are

$$F(E) = C(\epsilon, \lambda, T, \nu)M^2 \times \exp\left\{\frac{-h\nu_-}{2kT\lambda^2}\left[\frac{\nu}{2\nu_-} - (\lambda^2 + W)\right]^2\right\} \quad (19a)$$

$$\nu_{max} \approx \nu_-(\lambda^2 + W)\left[1 + \left(1 - \frac{8kT\lambda^2}{h\nu_-(\lambda^2 + W)^2}\right)^{1/2}\right] \quad (19b)$$

C is given by eq 14b and $\Delta\nu_{1/2}$ is the same as in eq 15. Again in the limit $h\nu_-\lambda^2 \gg kT$, noting then that $(h\nu_{max} - 2h\nu_-W) = 2h\nu_-\lambda^2$, one obtains the formula[4]

$$(h\Delta\nu_{1/2})^2 = 16kT \ln 2\,(h\nu_{max} - 2h\nu_-W) \quad (20)$$

Thus in the localized, high-temperature limit, a blue shift in ν_{max} of $2W\nu_-$ distinguishes the unsymmetrical case from its symmetrical counterpart.

A formula closely related to eq 19a has been derived by Hopfield using a different method.[5a] His results and eq 14, 15, and 19 will be compared with the PKS model in the next section.

IV. Predictions of the PKS Model. Comparisons with Earlier Formulas

The most important characteristics of an absorption band are its zeroth, first, and second moments, which measure respectively the integrated intensity, mean energy, and width. We investigate here the variation of these quantities with the PKS parameters (ϵ, λ, W) and the temperature, and we make comparisons with the semiclassical model and eq 14, 15, and 19.

We define the nth moment of $\alpha(E)$ about $\bar{E}$ by[7]

$$\langle\alpha\rangle_n^{\bar{E}} = \int_{band} \alpha(E)(E - \bar{E})^n \, dE \quad (21)$$

where $\bar{E}$ is the mean band energy defined by $\langle\alpha\rangle_1^{\bar{E}} = 0$. Thus

$$\bar{E} = \int \alpha(E)E \, dE / \int \alpha(E) \, dE \quad (22)$$

A theoretical absorption profile is defined by[7]

$$\alpha(E) = \sum_\gamma \sum_a \sum_j \frac{(N_a - N_j)}{N} |\langle a|m_\gamma|j\rangle|^2 f_{aj}(E) \quad (23)$$

where $\int f_{aj}(E)dE = 1$ and (N_a/N) and (N_j/N) are the fractional populations in states a and j. By substituting eq 23 into eq 21, *assuming a δ function line width for $f_{aj}(E)$*, explicit expressions for the desired moments have been obtained in the PKS model.[16] However, the density of lines in the model most certainly does not justify a δ function assumption. If this assumption is dropped, the zeroth-moment equation continues to apply, the first-moment equation applies only if $f_{aj}(E)$ is symmetrical about $(E_j - E_a)$, and the second-moment equation[16] can produce gross errors (see later).

We synthesized band contours by representing each line by a Gaussian whose area was proportioned to the (dipole) line strength and whose full width at half height was set uniformly at $2.4\nu_-$, with ν_- chosen arbitrarily as 450 cm^{-1}. This procedure[7] produces bands whose overall contour is fairly smooth, a characteristic of intervalence bands. The moments were obtained by numerically integrating the synthetic band contours in accord with eq 21 and 22. In all cases, the far-infrared transitions[8] were excluded, a matter of crucial importance since these can be very intense and would change the computed moments greatly. These are not a part of the intervalence band observed experimentally, and indeed their existence has yet to be experimentally confirmed.[8] The calculated zeroth and first moments are independent of the numerical value used for the line width, and they vary only slightly (less than 8% at 300 K) if ν_- is varied over the range 250–650 cm^{-1}. This is not the case for the second moment, and that point is discussed at the end of this section.

Moments for the semiclassical treatment are also given by eq 21. $\alpha(E)$ is simply identified with $F(E)$ (eq 12).

A. Integrated Band Intensity (Zeroth Moment). 1. Semiclassical Treatment. The simplest (and crudest) evaluation of eq 21 for $n = 0$ can be effected in the localized limit, $\lambda^2 \gg |\epsilon|$. In that case, the wells in the lower potential surface may be assumed sufficiently deep that only the transition from the

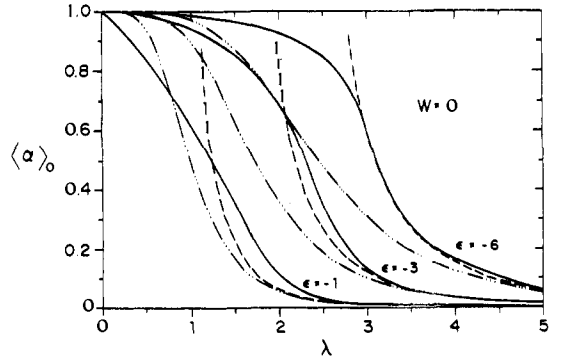

Figure 3. Plots of the zeroth moment ($\langle\alpha\rangle_0$) at 4.2 K, in units of M^2 vs. λ (with $W = 0$) for the PKS model (solid lines), eq 27 (dashed line), and eq 25 (dash-dot line).

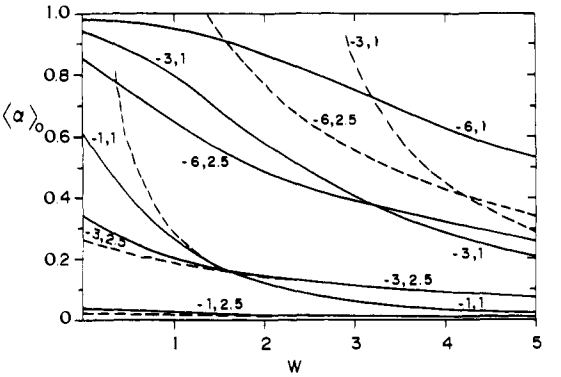

Figure 4. Plots of the zeroth moment ($\langle\alpha\rangle_0$) at 4.2 K, in units of M^2, vs. W for the PKS model (solid lines) and eq 27 (dashed lines). The parameters ϵ and λ label the curves. The dashed curve for −6.1 is off scale.

bottom contributes to eq 12. The zeroth moment thus becomes

$$\langle\alpha\rangle_0 = |\langle\psi_1|m_z|\psi_2\rangle|^2_{q=q_{min}} \tag{24}$$

where q_{min} is the value corresponding to the bottom of the well. Examination of eq 1 shows that for $\epsilon = 0$ (but for any value of W) $q_{min} = \pm\lambda$. (We follow the convention that W is always positive so that when $W \neq 0$, the lower of the two minima occurs at $q_{min} = +\lambda$ (see Figure 1).) Substituting $q_{min} = \lambda$ into eq 24 using eq 1, one obtains

$$\frac{\langle\alpha\rangle_0}{M^2} = \left[\frac{K(K + \sqrt{1 + K^2})}{1 + K\sqrt{1 + K^2} + K^2}\right]^2 \tag{25}$$

where $K \equiv |\epsilon|/(\lambda^2 + W)$. (For $|\epsilon| \neq 0$, $q_{min} = \lambda$ no longer applies exactly, but eq 25 is a limiting form for $\lambda^2 \gg |\epsilon|$.)

A better approach, clearly, is to evaluate eq 21 using eq 19; however, we must first eliminate the singularity in $F(E)$ (see Figure 2). To do this, we again note that $C(\epsilon, \lambda, T, \nu)$, eq 14b, is a relatively weak function of frequency in the region of strong absorption. We therefore set $\nu = \nu_{max} \approx 2(\lambda^2 + W)\nu_-$ in C. The effect of this approximation, which becomes steadily better as $(\lambda^2 + W)$ becomes large compared to $|\epsilon|$, is shown for two cases in Figure 2. $F(E)$ becomes exactly Gaussian, and its zeroth moment can be written

$$\frac{\langle\alpha\rangle_0}{M^2} = K^2(1 - K^2)^{-1/2} \exp(K'\epsilon^2/\lambda^2) \tag{26}$$

where $K \equiv |\epsilon|/(\lambda^2 + W)$ and $K' \equiv h\nu_-/2kT$. Consistent with our semiclassical treatment, eq 26 should be valid only if $K'\epsilon^2/\lambda^2 \ll 1$. Consequently, in the localized, high-temperature limit

$$\frac{\langle\alpha\rangle_0}{M^2} = K^2(1 - K^2)^{-1/2} \tag{27}$$

2. Results and Comparisons. Plots of $\langle\alpha\rangle_0/M^2$ vs. λ and W using eq 25 and 27 and the PKS model are shown for a few selected parameters in Figures 3 and 4. All results agree in the localized limit (i.e., in the limit of strong vibronic coupling, $\lambda^2 + W \gg |\epsilon|$). As expected, the results based on eq 27 have a greater range of validity than those based on eq 25. The latter does have the feature of being correct at $\lambda = 0$ if $W = 0$, but this does not have a theoretical significance. Again, as expected, the semiclassical and PKS models diverge as $|\epsilon|$ increases.

Examining Figure 3, we see that the PKS model predicts a sharp decrease in $\langle\alpha\rangle_0$ as λ increases, the region of most rapid change occurring a little after the change from the delocalized to localized case ($\lambda^2 = |\epsilon|$). From Figure 4 we see that $\langle\alpha\rangle_0$ drops off steadily with increasing W.

Figure 5 shows the predicted temperature dependence of

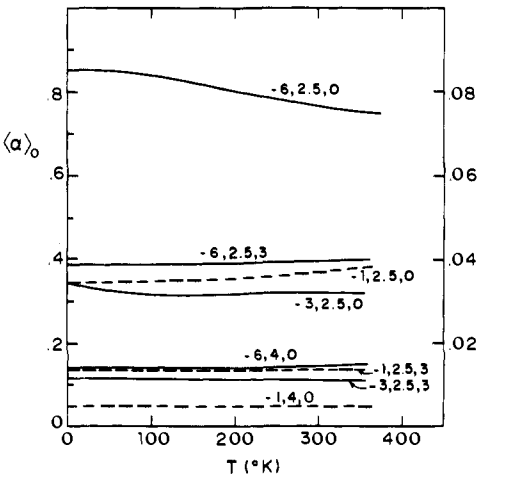

Figure 5. Plots of the zeroth moment ($\langle\alpha\rangle_0$) in units of M^2 vs. temperature for the PKS model. The parameters ϵ, λ, W label the curves. The left-hand ordinate applies for the solid lines, and the right-hand ordinate applies for the dashed lines.

$\langle\alpha\rangle_0$ according to the PKS model for some selected parameters. The striking point is the extreme *insensitivity* to temperature *in all cases*, the greatest variation observed (for $\epsilon = -6$, $\lambda = 2.5$, $W = 0$) being less than 10% between 0 and 400 K. Unless base lines of exceptional reliability can be measured, changes of this magnitude will be undetectable, and so the PKS model predicts negligible temperature dependence for the intervalence band area.

B. Mean Band Energy (First Moment). 1. Semiclassical Treatment. Proceeding as with the zeroth moment, in the strong vibronic coupling (i.e., localized) limit ($\lambda^2 + W \gg |\epsilon|$), the crudest approximation to the mean band energy is simply the vertical excitation from the bottom of the well(s) in the lower potential surface to the upper surface. From the expressions for E_1 and E_2, eq 1, it follows that

$$E_{vert} = E_{op} \approx \bar{E} = 2(\lambda^2 + W)h\nu_- \tag{28}$$

A better alternative is to choose $\bar{E} = E_{max}$ in accord with eq 19. This would be an exact relationship if $F(E)$ (eq 19) were exactly Gaussian. Thus for the semiclassical treatment we write

$$\bar{E} \approx E_{max} = (\lambda^2 + W)h\nu_-\left[1 + \left(1 - \frac{8kT\lambda^2}{h\nu_-(\lambda^2 + W)^2}\right)^{1/2}\right] \tag{29}$$

which reduces to eq 28 for $(\lambda^2 + W)/kT$ sufficiently large, i.e.,

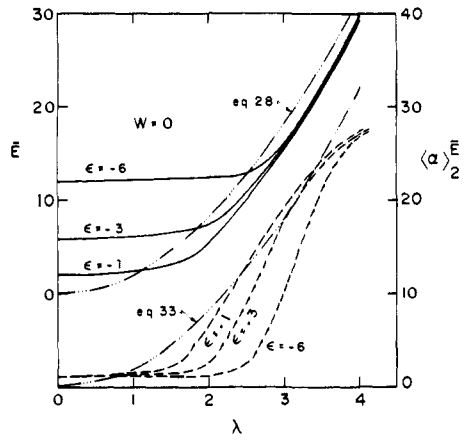

Figure 6. Plots of the first ($\bar{E}$) and second ($\langle\alpha\rangle_2^{\bar{E}}$) moments vs. λ at 4.2 K with $\nu_- = 450$ cm^{-1} and for Gaussian line widths (at half height) of 2.4 ν_-. $\bar{E}$ and $\langle\alpha\rangle_2^{\bar{E}}$ are respectively in units of $h\nu_-$ and $M^2(h\nu_-)^2$. The solid and dashed curves are respectively $\bar{E}$ (left ordinate) and $\langle\alpha\rangle_2^{\bar{E}}$ (right ordinate) for the PKS model. The dash-dot curves apply for the indicated equations which have no ϵ dependence.

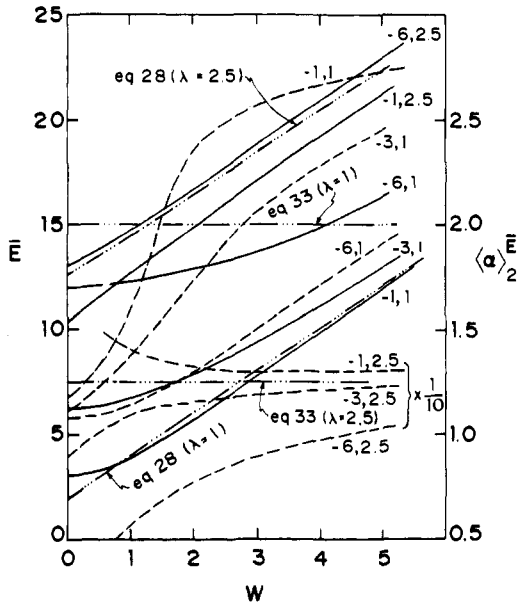

Figure 7. Plots of the first and second moments vs. W. Notation and conditions are as in Figure 6. The parameters ϵ, λ label the curves. For those curves labeled $\times$ 1/10, the ordinate scale should be multiplied by 10.

for sufficiently strong vibronic coupling and/or sufficiently low temperature.

2. Results and Comparisons. Figures 6 and 7 show the variation of the first moment (solid lines) with λ and W for $|\epsilon| = 1, 3, 6$. Once again it is seen that the semiclassical treatment (eq 28) agrees very well with the PKS model as ($\lambda^2 + W$) becomes large compared to $|\epsilon|$. In the delocalized case ($\lambda^2 + W \lesssim |\epsilon|$), however, the discrepancies can become very large. Analogous remarks apply for the temperature dependence (Figure 8). The semiclassical treatment approaches PKS for large λ and high temperatures; it also predicts a blue shift with decreasing temperature, and the magnitude of the effect is considerably greater than by PKS, which indeed sometimes predicts a red shift. As with the zeroth moment, the effect of temperature is predicted by the PKS model to be small in all cases.

C. Bandwidth (Second Moment). 1. Semiclassical Treatment. The second moment may be written down immediately since, consistent with the assumption of a Gaussian band in obtaining

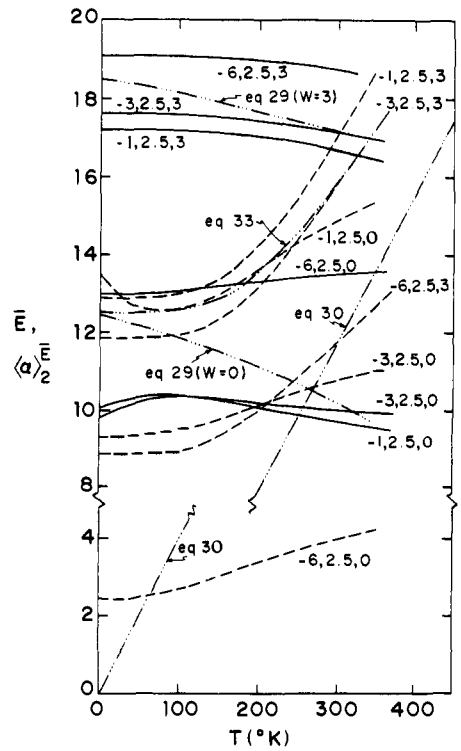

Figure 8. Plots of the first and second moments vs. temperature. Notation and other conditions are as in Figure 6. The parameters ϵ, λ, W label the curves. ($\lambda = 2.5$ in all cases.) Equations 30 and 33 are independent of both ϵ and W while eq 29 is independent of ϵ.

eq 15, $\Delta\nu_{1/2}$ is simply related to the second moment:

$$\frac{\langle\alpha\rangle_2^{\bar{E}}}{M^2(h\nu_-)^2} = (\Delta\nu_{1/2})^2/8 \ln 2 = 4\lambda^2\left(\frac{kT}{h\nu_-}\right) \qquad (30)$$

Equation 30, in effect, is the relation used in deriving eq 18 and 20.

2. The Delocalized Treatment of Reference 6 ($|\epsilon| \gg \lambda^2$). The following formula has been proposed[6] for a symmetrical system (A = B) in the delocalized case:

$$\Delta\nu_{1/2} = (4 \ln 2)^{1/2} \times \theta(1-\theta)^{-1/2}\,\nu_-\coth\left(\frac{h\nu_-(1-\theta)^{1/2}}{2kT}\right) \qquad (31)$$

where $\theta \equiv \lambda^2/|\epsilon|$. No derivation of this formula was given, but reference was made to the work of Kubo and Toyozawa.[17] We here sketch a derivation which makes it clear that eq 31 has very limited applicability to mixed-valence systems.

As discussed in section II, if $\lambda = 0$, the two potential surfaces are identical, vertically displaced parabolas (Figure 1f), and so eq 3 applies with χ_m and $\chi_{m'}$ members of the same set of harmonic oscillator functions. Application of the Franck-Condon principle (valid in this limiting case) leads immediately to the prediction that the intervalence band consists of a single line whose width and intensity are *independent of temperature*. Let us assume (incorrectly!), when $\lambda^2 \neq 0$ but $\ll |\epsilon|$, that the potential surfaces remain parabolas. Let us also assume (incorrectly) that solutions in the Born-Oppenheimer form (eq 3) continue to apply and that the Franck-Condon approximation can be made. Then the force constant for each potential surface is obtained by evaluating the second derivative at the potential minimum. Using eq 1, one obtains $k_1 = 1 - \theta$, $k_2 = 1 + \theta$. Evaluating the second moment (eq 21 for $n = 2$) using eq 23 with $f_{aj} = \delta_{aj}$, the result is (see Appendix)

$$\langle\alpha\rangle_2^{\bar{\nu}} = \left(\frac{M^2}{8}\right)\nu_1^2\left(\frac{k_2 - k_1}{k_1}\right)^2 \coth^2\left(\frac{h\nu_1}{2kT}\right) \qquad (32)$$

If one now defines ν_- by $\nu_1 = (\nu_-)\sqrt{k_1}$, $\nu_2 = (\nu_-)\sqrt{k_2}$, and notes that for a *Gaussian* band $\langle\alpha\rangle_2^{\bar{\nu}} = (\Delta\nu_{1/2})^2/8 \ln 2$, eq 31 (in units of M) results. We shall find in part 4 of this section that eq 31 has no quantitative applicability.

3. The Result in the Localized Limit ($\lambda^2 + W \gg |\epsilon|$). If $\epsilon = 0$ (Figure 1b), eq 3 applies; the two potential surfaces are parabolas and the Franck-Condon approximation can be made. It is then possible to calculate the second moment in a straightforward manner. The result is (see Appendix)

$$\frac{\langle\alpha\rangle_2^{\bar{E}}}{M^2(h\nu_-)^2} = 2\lambda^2 \coth\left(\frac{h\nu_-}{2kT}\right) \tag{33}$$

Although $M \approx 0$ if ϵ is precisely zero,[7] eq 33 should be a reasonable approximation when $\lambda^2 + W \gg |\epsilon| \neq 0$. Equation 33 reduces to eq 30 when $2kT \gg h\nu_-$. An expression similar to eq 33 was employed by Atkinson and Day to fit their experimental data.[23]

4. Comparisons with the PKS Model. Referring to Figure 6, we see the variation of the second moment with λ for the localized case (eq 33) and for the PKS model (dashed lines). As expected, eq 33 and the PKS model converge as λ^2 becomes large compared to $|\epsilon|$. On the other hand, eq 31, which is supposed to be valid for small θ ($\equiv \lambda^2/|\epsilon|$), predicts that the second moment should vary as $\theta^2/(1-\theta)$ and thus should be a strong function of both λ and ϵ as $\theta \to 0$. The PKS model is seen to predict just the opposite. In Figure 7, we see the variation of the second moment (dashed lines) with W for the PKS model. It generally increases with W except in the strongly localized case ($\epsilon = -1$, $\lambda = 2.5$) where an actual decrease is predicted. The semiclassical formula, eq 30 (and its low-temperature counterpart, eq 33), predicts no W dependence. Consistent with this, the PKS model shows a leveling off as ($\lambda^2 + W$) increases.

Finally, in Figure 8 we see the variation in second moment with temperature. Results are shown for the PKS model (dashed lines) and for eq 30 and 33. A monotonic increase in second moment with temperature is predicted in all cases except in the PKS model for $\epsilon = -1$, $\lambda = 2.5$, $W = 0$, where there is a small initial decrease. As might be expected, eq 33 agrees quite well with the PKS model in the strongly localized cases. Interestingly, the PKS model predicts the strongest temperature dependence in the transition region between the localized and delocalized cases ($\lambda^2 \approx |\epsilon|$). Thus in the case $\epsilon = -6$, $\lambda = \sqrt{6}$, the second moment ratio SM(350 K)/SM(0 K) = 1.73, whereas eq 33 gives a ratio of 1.49. The physical reason for this behavior is qualitatively clear from Figure 1e. It is seen that, at $\lambda^2 = |\epsilon|$, the bottom potential surface becomes wide and flat. Hence a large broadening of the band will occur as higher vibronic states are thermally populated. It is also seen that the second moment has an inflection point for $\lambda^2 = |\epsilon|$ around 200 K, and hence the behavior is qualitatively quite different from eq 33. (This behavior is also observed in the localized case as states close to the top of the barrier become thermally populated.) As one moves to more delocalized systems ($|\epsilon| > \lambda^2$), the temperature dependence falls off and goes to zero in the delocalized limit ($|\epsilon| \gg \lambda^2$). Equation 30 is not very useful except as an asymptote at very high temperatures ($T \gtrsim 500$ K) for the case ($\lambda = 2.5$) shown in Figure 8. As λ gets larger, the temperature at which eq 30 becomes useful drops. However, more to the point, eq 33 is always preferable to eq 30 because it has the same asymptotic behavior (at high temperature) and should always better approximate the experimental behavior at lower temperatures. Since eq 30 and 33 have no ϵ dependence, they are grossly in error in absolute magnitude when $|\epsilon|$ becomes large.

Equation 31 is qualitatively correct in predicting that the intervalence band will become sharper with increasing delocalization, but, as indicated above, its behavior as a function of $|\epsilon|$ and λ is incorrect as $\theta \to 0$, and it clearly cannot be correct in the region of the crossover to the localized case ($\theta = 1$). It is also qualitatively correct in predicting that the bandwidth will increase more slowly with temperature as a system becomes more delocalized. However, it is again markedly incorrect in the delocalized limit ($\theta \to 0$) since it predicts then that $\Delta\nu_{1/2} \sim \coth(h\nu_-/2kT)$, whereas the standard Franck-Condon argument cited in part 2 of this section requires that $\Delta\nu_{1/2}$ be *independent* of temperature in this limit. The use[6] of eq 31 for the Creutz and Taube complex depended on an unrealistic choice of ν_- ($\sim$800 cm^{-1}) corresponding to a rocking frequency, whereas a value of about 500 cm^{-1} is appropriate.[7]

Hopfield,[5a] working in the localized limit and using a different method, has derived an expression for the intervalence band contour (his eq 17) which closely resembles our eq 19a. Indeed, if $\Delta\nu_{1/2}$ is identified with eq 33 rather than eq 30, and if, in our eq 14b, the exponential is set equal to unity *and* ν is set equal to $\nu_{max} = 2\nu_-(\lambda^2 + W)$—both excellent approximations in the localized limit—then the Hopfield eq 17 and our eq 19a are essentially identical. The following relations apply between the Hopfield parameters T_{da}, Δ, and ($E_a - E_d$) and ours: $T_{da} = -\epsilon h\nu_-$, $\Delta = 2\lambda^2 h\nu_-$, and $(E_a - E_d) = 2Wh\nu_-$. The parameters of Potasek and Hopfield[5b] for the model system cytochrome c-Fe(CN)$_6$ translate in our nomenclature to $\epsilon = -0.04$, $\lambda = 3.96$, $W = 2.1$, and $h\nu_- \approx 250$ cm^{-1}, and these clearly describe a strongly localized system, fully consistent with the Hopfield model.[5a]

As indicated earlier, for the PKS model the $\langle\alpha\rangle_0$ and $\bar{E}$ results presented in Figures 3-8 are, to a very good approximation, independent of the values used for the line width and ν_-. This is not true for the second moments. One finds that the variation with ν_- is not great and is systematic. Thus the second moment varies $\sim(1/\nu_-)$ for localized systems, as predicted by eq 30, and this dependence levels off as $|\epsilon|$ approaches $\lambda^2 + W$. For example, at 300 K over the ν_- range 300-600 cm^{-1}, the second moment decreased by about 30% for $\epsilon = -1$, $\lambda = 4$, $W = 3$, by about 20% for $\epsilon = -1$, $\lambda = 4$, $W = 0$, and by about 4% for $\epsilon = -6$, $\lambda = 1$, $W = 3$. The second moment is a sensitive function of the line width in the delocalized case, but the effect becomes much less pronounced as ($\lambda^2 + W$) increases. For example, when $\nu_- = 450$ cm^{-1}, $T = 4.2$ K, and the line width is varied from $1.2\nu_-$ to $4.8\nu_-$, one finds for $\epsilon = -6$, $\lambda = 2.5$, $W = 0$ that the second moment increases from 1.6 to 5.9, but for $\epsilon = -1$, $\lambda = 3$, $W = 0$ the increase is only from 18.0 to 25.3. Thus, while the systematic trends for the second moments are perfectly valid in Figures 6-8, if a comparison is made with a real band, it is necessary to use a reasonable value for ν_- and to choose the line width parameter to give a good fit of the overall band contour.

If δ function line widths are assumed,[16] second moments calculated with the PKS model will in general be far smaller than those for real bands because of the sparsity of lines inherent in the model.

A summary of the range of validity of the formulas discussed in this section is presented in section IX.

V. Degree of Delocalization

In earlier sections, the localized and delocalized cases have been distinguished by the criteria $\lambda^2 + W > |\epsilon|$ vs. $|\epsilon| > \lambda^2 + W$, and we have noted that the barrier in the lower potential surface just disappears at $\lambda^2 = |\epsilon|$ (for $W = 0$). Moreover, it is clear qualitatively (Figure 1) and on physical grounds that increasing W always favors localization. It is possible to formulate quantitative criteria to describe the degree of delocalization. We do this first using a static model. This leads, in the localized limit, to an expression (eq 40) previously cited in the literature. We then propose an expression based on the PKS model.

A. Static Model. Rewriting eq 1 in terms of $\psi_a = \psi_M{}^A\psi_N{}^B$ and $\psi_b = \psi_N{}^A\psi_M{}^B$, one obtains

$$\psi_1 = -\frac{1}{N\sqrt{2}}[(\epsilon - \kappa + \sigma)\psi_a + (\epsilon - \kappa - \sigma)\psi_b]$$

$$\psi_2 = \frac{1}{N\sqrt{2}}[-(\epsilon - \kappa - \sigma)\psi_a + (\epsilon - \kappa + \sigma)\psi_b] \quad (34)$$

where N, κ, and σ, defined just below eq 1, are functions of q. If $\epsilon = 0$, $\kappa = \sigma$ and $N = \sigma\sqrt{2}$ so that $\psi_1 = \psi_b$ and $\psi_2 = \psi_a$. This is consistent with an intuitive picture of complete localization since there is no mixing of the two "monomer" wave functions. When $\epsilon \neq 0$, electronic interaction occurs, and we symbolize the square of the coefficient of ψ_a in ψ_1 as $\alpha_d{}^2(q)$. Thus

$$\alpha_d{}^2(q) = \frac{(\epsilon - \kappa + \sigma)^2}{2N^2} \quad (35)$$

An examination of eq 1 shows that, for $\epsilon = 0$, $W \neq 0$, the minima in the lower potential surface (E_1) occur at $q = \pm\lambda$. In the spirit of the semiclassical approach, we set $q = \lambda$ in eq 35 and accordingly *define* the degree of delocalization by $\alpha_d{}^2 \equiv \alpha_d{}^2(q = \lambda)$. By straightforward algebra

$$\alpha_d{}^2 = \frac{1}{2}\left[1 - \left\{\frac{(\lambda^2 + W)^2}{\epsilon^2 + (\lambda^2 + W)^2}\right\}^{1/2}\right] \quad (36)$$

This quantity is meaningful only for localized systems; for $\epsilon^2/(\lambda^2 + W)^2 \ll 1$

$$\alpha_d{}^2 = \frac{1}{4}\frac{\epsilon^2}{(\lambda^2 + W)^2} \quad (37)$$

We can relate this result to experimental observables by using eq 27 so that

$$\alpha_d{}^2 \approx \frac{1}{4}\frac{\langle\alpha\rangle_0}{M^2} \quad (38)$$

Using[7]

$$M^2 = (gRe/2)^2 \quad (39)$$

where R is the distance between monomer centers, e is the electronic charge, and g is the difference in oxidation state of the two monomers, eq 38 can be written[4b]

$$\alpha_d{}^2 = \frac{3.983 \times 10^{-4}}{R^2}\langle\alpha\rangle_0 = \frac{4.24 \times 10^{-4}\,\epsilon_{max}\,\Delta\nu_{1/2}}{\nu_{max}R^2} \quad (40)$$

for $g = 1$, where dipole moments are expressed in debye and R is in ångstroms. In eq 40, ϵ is the molar extinction coefficient (not to be confused with ϵ of the PKS model!), $\Delta\nu_{1/2}$ and ν_{max} are in the same units, and the last expression in eq 40, frequently cited in the literature,[18] applies for a Gaussian band. $\alpha_d{}^2$ *ratios* calculated from eq 40 for related compounds in the localized limit may be useful, but actual numerical values for individual compounds are devoid of significance because eq 39 grossly overestimates experimental transition dipole strengths.[8] *Consequently, degrees of delocalization calculated using eq 40 are absurdly small.*

B. The PKS Model. Starting with eq 8, let us examine the expression obtained if $|\Phi_\nu|^2$ is integrated over the vibrational coordinate, q, i.e.

$$P_\nu(\text{el}) \equiv \int|\Phi_\nu|^2 dq$$

$$= \frac{1}{2}(\psi_a{}^2 + \psi_b{}^2) + (\psi_a{}^2 - \psi_b{}^2)\sum_{n=0}^{\infty} r_{\nu n}\, r'_{\nu n} + \psi_a\psi_b\sum_{n=0}^{\infty}(r_{\nu n}{}^2 - r'_{\nu n}{}^2) \quad (41)$$

In obtaining eq 41, use is made of eq 2, the fact that $\langle\chi_n|\chi_{n'}\rangle = \delta_{nn'}$, and the normalization condition, $\Sigma_n(r_{\nu n}{}^2 + r'_{\nu n}{}^2) = 1$. In the symmetrical ($W = 0$) case, eq 41 simplifies to

$$P_\nu{}^+(\text{el}) = \frac{1}{2}(\psi_a{}^2 + \psi_b{}^2) + \psi_a\psi_b\left(\sum_{\substack{n=0,2,\\4,\ldots}}^{\infty} r_{\nu n}{}^2 - \sum_{\substack{n=1,3,\\5,\ldots}}^{\infty} r_{\nu n}{}^2\right) \quad (42)$$

($P^-{}_\nu$(el) is obtained from eq 42 by replacing $r_{\nu n}$ by $s_{\nu n}$ and interchanging the two sums in the last term.) $\psi_a{}^2 = |\psi_M{}^A\psi_N{}^B|^2$ represents the probability of simultaneously finding center A in oxidation state M and center B in oxidation state N, and $\psi_b{}^2 = |\psi_N{}^A\psi_M{}^B|^2$ represents the reverse. These probabilities are equal in the symmetric (A = B) case (first term, eq 42). In the unsymmetrical case, the weightings will be different (first *two* terms, eq 41). Thus we may define a dissymmetry factor

$$\gamma_{dis}(\nu) \equiv \frac{1 - 2\left|\sum_n r_{\nu n}\, r'_{\nu n}\right|}{1 + 2\left|\sum_n r_{\nu n}\, r'_{\nu n}\right|} \quad (43)$$

$\gamma_{dis} = 1$ is the symmetrical limit (A = B), and smaller values reflect the disymmetry ($W \neq 0$); $\gamma_{dis} = 0$ represents the extreme case in which each center is characterized by only one oxidation state.

The term which measures delocalization is $\psi_a\psi_b = (\psi_M{}^A\psi_N{}^A\psi_M{}^B\psi_N{}^B)$, and we *define* the degree of delocalization in state ν ($\beta_d{}^2(\nu)$) by the square of the $\psi_a\psi_b$ coefficient, eq 41 (or eq 42):

$$\beta_d{}^2(\nu) \equiv \left[\sum_n (r_{\nu n}{}^2 - r'_{\nu n}{}^2)\right]^2 \quad (44)$$

If several states are thermally populated, γ_{dis} and $\beta_d{}^2$ will be given by the thermal averages of eq 43 and 44:

$$\overline{\gamma_{dis}} = \sum_\nu N_\nu\,\gamma_{dis}(\nu)\Big/\sum_\nu N_\nu$$

$$\overline{\beta_d{}^2} = \sum_\nu N_\nu\,\beta_d{}^2(\nu)\Big/\sum_\nu N_\nu \quad (45)$$

where $N_\nu = \exp(-E_\nu/kT)$.

One may obtain β_d in the localized limit as the coefficient of $\psi_a\psi_b$ in $\psi_1{}^2$, eq 34. If this is done and terms of order $\epsilon^4/(\lambda^2 + W)^4$ and higher are discarded, then $\beta_d{}^2 = \epsilon^2/(\lambda^2 + W)^2 = 4\alpha_d{}^2$ (by eq 37). Thus $4\alpha_d{}^2$ is the quantity which should be compared with $\overline{\beta_d{}^2}$. In Figure 9, plots of $\overline{\beta_d{}^2}$, $4\alpha_d{}^2$, and $\overline{\gamma}_{dis}$ are shown as a function of the various parameters. $4\alpha_d{}^2$ and $\overline{\beta_d{}^2}$ agree in the localized limit and diverge as the ratio $|\epsilon|/(\lambda^2 + W)$ increases. Interestingly, $\overline{\beta_d{}^2}$ closely parallels $\langle\alpha\rangle_0$ for the PKS model over the entire range of parameters (compare Figures 9 and 3), as does $4\alpha_d{}^2$ in the localized limit (eq 38). In fact, in most cases, $M^2\overline{\beta_d{}^2}/\langle\alpha\rangle_0 = 1.0 \pm 0.1$. Thus the integrated intervalence band intensity will serve as a reasonable measure of the degree of delocalization in a series of related compounds. For the parameters used in Figure 9, the temperature dependence of $\overline{\beta_d{}^2}$ and $\overline{\gamma}_{dis}$ is negligible. Thus in this case we need not distinguish between $\overline{\beta_d{}^2}$ and $\beta_d{}^2$, etc.

$\overline{\gamma}_{dis}$ behaves in the expected way and may prove a useful quantity in characterizing the unsymmetrical case.

VI. Extracting Parameters from Experimental Data

In the PKS model, the parameters, ϵ, λ, and W ($W = 0$ for the symmetrical case) determine the complete set of eigenfunctions for the ground vibronic manifold of a mixed-valence system. Consequently, if these parameters are known, observable properties of the system can be calculated in a straightforward way. In this paper, we have concentrated on the spectroscopic properties of the intervalence band, but we note that a plot of the probability distribution in q space gives a *quantitative picture* of the degree of delocalization as a

function of temperature (Figure 4, ref 7). ϵ, λ, and W also define the potential surfaces of the system (Figure 1). On the other hand, the simple expression obtained for the electric dipole transition matrix element, eq 39, is devoid of quantitative significance, and *absolute* intensities must be determined experimentally. ν_-, the fundamental frequency of vibrational mode q, must also be determined from experiment, but a reasonable estimate is usually possible from known vibrational data.

It seems clear, therefore, that a great deal of interesting chemical information can be obtained from the intervalence band if the parameters, ϵ, λ, and W can be reliably extracted from the band contour. This should be possible, especially if series of related compounds are analyzed.

The obvious procedure is to determine the parameters by fitting the band contour. In the case of the Creutz and Taube complex, this proved possible[7] with a surprising degree of uniqueness, $\epsilon = -6.0 \pm 0.1$, $\lambda = 2.7 \pm 0.2$. When similar procedures were used[8] on the related compound **2**, the fit of the band

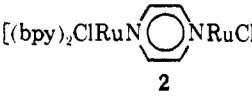

2

contour was not as good, and two ranges of values of the parameters seemed possible. However, the previous analysis of the Creutz and Taube complex permitted a choice to be made. Since molar extinction coefficients had been reported for both compounds, it was possible, first of all, to determine M^2 for the Creutz and Taube complex from the experimental band area (zeroth moment). (In fact, the result can be read off Figure 3 by noting the ordinate corresponding to $\epsilon = -6$, $\lambda = 2.7$.) Assuming that **2** is sufficiently similar that roughly the same M value is applicable, it is possible from the experimental zeroth moment to distinguish clearly between the two alternative parameter sets, since one set ($\epsilon \sim -3$, $\lambda \sim 3$) predicted approximately the observed band intensity,[8] and the other set ($\epsilon \sim -7$, $\lambda \sim 2.7$) predicted a band intensity about seven times greater. This illustrates the utility of studying related compounds and emphasizes the very great importance of measuring molar extinction coefficients and accurate band contours.

The success of such procedures, particularly in $W \neq 0$ cases, requires systematic investigation and can draw on the considerable data already in the literature. Figures 3-8 give cause for optimism on this score. Zeroth moments (integrated intensities) can be used in the manner already indicated. Furthermore, unlike the zeroth moment, the first and second moments (Figures 6-8) are absolute numbers (in ν_- quanta) and may vary very widely as a function of ϵ, λ, and W.

The weak temperature dependence of the zeroth and first moments suggest that such data will not be very useful. However, accurate second-moment measurements as a function of temperature may prove valuable. As a practical matter, use of a digital computer can make fitting procedures simple and straightforward. First, the diagonalizations required to solve the secular equations (eq 5 or 9) are simple and economical. Second, with the use of relatively simple interactive graphics, one can very quickly explore fits of an experimental band over a wide range of parameters. Thus one can ascertain the uniqueness of a fit and determine whether further criteria, such as absolute intensity or temperature-dependence information, is required. Having obtained the parameters ϵ, λ, and W, the subsequent calculation of quantities such as the probability distribution in q space, potential surfaces, $\overline{\beta_d{}^2}$, $\overline{\gamma}_{dis}$, or the predicted spectrum at other temperatures becomes trivial.

If it has been established that one is dealing with a strongly localized system ($\lambda^2 + W \gg |\epsilon|$), then, of course, analytical formulas are available. These are summarized in Table I, section IX. Again, Figures 3-8 provide guidance as to the range of validity of such relationships.

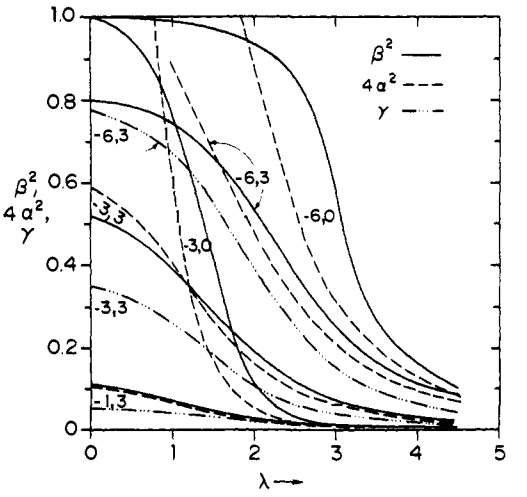

Figure 9. Degree of delocalization for the PKS (solid line, $\overline{\beta_d{}^2}$) and static models (dashed line, $4\alpha_d{}^2$ by eq 36), and dissymmetry factor for the PKS model (dash-dot line, $\overline{\gamma}_{dis}$), all as a function of λ. The parameters ϵ, W label the curves. For the parameters shown, $\overline{\beta_d{}^2}$ and $\overline{\gamma}_{dis}$ have negligible temperature dependence from 0 K to room temperature.

VII. Classification of Mixed Valence Systems

The classification scheme of Robin and Day,[2] mentioned at the beginning of this article, may readily be recast and refined using the parameters ϵ, λ, and W. Thus compounds in classes[2] I, II, and III correspond respectively to the cases $|\epsilon| \ll (\lambda^2 + W)$, $|\epsilon| \lesssim (\lambda^2 + W)$, and $|\epsilon| > (\lambda^2 + W)$. Robin and Day based their classification primarily on a parameter, E_ℓ, which is roughly equivalent to our W. By inspection of Figures 1 and 3-9, we observe the following. Class I compounds are strongly localized (valence trapped); the intervalence band tends to high energy and large width and is of low or negligible intensity. Class III compounds are completely delocalized; the intervalence band tends to low energy, small width, and high intensity. Class II compounds are intermediate; there is some delocalization, but valences are still distinguishable (valence trapped). This, in fact, requires a small potential barrier in the lower potential surface. To distinguish this case from class III, one need only make a probability plot in q space (Figure 4, ref 7). Whether a single or double maximum occurs distinguishes respectively the class III and class II cases. It is interesting to note that by this criterion, according to the PKS analysis,[7] the Creutz and Taube complex is borderline between classes II and III. The potential barrier in the lower surface is small ($\sim$57 cm^{-1}); at low temperature there is no trapping, but at room temperature the probability distribution shows two slight maxima.[7]

The basic difference between the Robin and Day and PKS classification criteria is the fact that the former was framed in terms of a single parameter (E_ℓ) and hence does not explicitly include the role of either electronic or vibronic coupling; the latter includes both of these effects. However, the PKS model, as presently formulated,[7] applies only to two interacting centers; the Robin and Day classification, though obviously much more qualitative, also includes metal cluster systems. Furthermore, whereas E_ℓ is used to describe the case when two metal centers have different symmetries, the use of W in such a context is qualitative at best since the PKS model would require substantial modification to treat such systems. Also inherent in the Robin and Day scheme is the notion that, if the two ions (in different oxidation states) are in exactly equivalent sites ($E_\ell = 0$), then the system is completely delocalized. This

Table I. Status of Formulas in Text

text eq no.	range of validity	comments
31[a]	no quantitative validity	See section IVC2.
15,[a] 16b,[a] 18,[a] 20,[a] 25, 30,[a] 36,[b] 37,[b] 38, 40[a,b]	strongly localized systems; $(\lambda^2 + W) \gg \lvert\epsilon\rvert$	Equations 18 and 20 would be significantly improved if eq 33[c] were used instead of eq 15. Equation 25 behaves correctly in the delocalized limit. Equation 40 is grossly in error in absolute value (section VA).
27, 28,[a] 29, 33[a]	localized systems; $(\lambda^2 + W) > \lvert\epsilon\rvert$	Equation 33[c] is always better than its high-temperature counterparts, eq 30 and 15.
16a,43, 44,[b] 45[b]	general; i.e., applicable for all ϵ, λ, W	

[a] Used in the previous mixed-valence literature. [b] $4\alpha_d^2$ is the quantity comparable to β_d^2 (or $\overline{\beta_d^2}$). [c] For a Gaussian, $(\Delta\nu_{1/2})^2 = (8 \ln 2)\langle\alpha\rangle_2^{\bar{r}}$.

applies also in our scheme if exactly equivalent sites means $W = 0$ *and* $\lambda = 0$. If only the former is true (the PKS symmetrical A = B case), the degree of delocalization can span the full range. It is determined primarily by the ratio $|\epsilon|/\lambda^2$, and can be calculated as discussed in section V.

VIII. Extension of the Model and Other Applications

Several extensions of the PKS model seem feasible. One should be able to include several interacting "monomers", the simplest case probably being a linear chain. There is considerable interest in such systems.[3,19] Examination of the case in which the two "monomers" have different local symmetries would also clearly be of interest. In addition, analysis of the consequences of relaxing some of the restrictive assumptions of the model would be illuminating, e.g., the assumption of identical force constants in all cases, the assumption of identical vibronic coupling in both monomer units in the unsymmetrical case, and the assumption of a purely electronic coupling between the two monomers.

One interesting application of the model which we shall describe elsewhere is the analysis of spin crossover systems. If we imagine a molecule with two different spin states coupled by a totally symmetric molecular vibration (i.e., within the amplitude of the vibration, one changes spin states), then one can anticipate vibronic effects which might affect magnetic properties. Indeed, one can immediately treat such a system with the PKS model by simply reidentifying the parameters and translating the coordinate origin. W becomes the difference in zero point potential energy of the two spin states, ϵ is directly proportional to the spin-orbit interaction between them, and λ measures the difference in equilibrium value of the a_{1g} coordinate in the two spin states. Our calculations to date, using a model system, indicate that the resulting vibronic effects can alter such properties as the magnetic susceptibility of the system.

Finally, we stress that, although the mixed-valence concept is usually applied to the coupling of transition-metal ions in different oxidation states, and our specific applications have been to such systems,[7,8] the PKS model has potential applicability to any system containing relatively weakly coupled subunits in different oxidation states. Specifically, if the electronic coupling, vibronic coupling and monomer zero-point energies are not too disparate, and if all are relatively small compared to subunit electronic excitation energies, then a relatively low energy intervalence band may be anticipated which can be characterized by the parameters ϵ, λ, and W. Such a band, for example, appears to have been observed[20] around 900–1000 nm in benzene and naphthalene dimer cations, $(C_6H_6)_2^+$ and $(C_{10}H_8)_2^+$. These systems would constitute the symmetrical (A = B) case, the two formal oxidation states in $(C_6H_6)_2^+$, for example, being represented by C_6H_6 and $C_6H_6^+$.

Note Added in Proof. We have fit the band at ~926 nm[20] in $(C_6H_6)_2^+$ using the PKS model. Choosing $\nu_- = 991$ cm^{-1} (the benzene a_{1g} ring stretching mode), we obtain $\epsilon = -5.0 \pm 0.1$, $\lambda = 2.5 \pm 0.1$ (and $W = 0$). This corresponds formally to the localized case but with a barrier in the lower potential surface of only about 125 cm^{-1} which is about 60 cm^{-1} *below* the lowest vibronic level. The parameters predict a far-infrared "tunneling" transition[8] at about 265 cm^{-1} with an integrated intensity about 40% that of the 926-nm band.

IX. Conclusions. Validity of Various Formulas

As we have emphasized previously,[7] the PKS treatment itself provides a simplified model of mixed-valence systems. Nevertheless, the model is clearly defined and treats the vibronic and electronic coupling using well-recognized quantum mechanical techniques.[11] The model quite clearly accounts for many of the properties of mixed-valence systems and is amenable to further refinement and generalization. Furthermore, a variety of formulas which have been widely used in the literature are obtained as well-defined limiting cases of this model. Thus it is possible to put earlier results in a context in which their limitations can be clearly understood. We summarize in Table I the status of various formulas which have been derived in this paper including those used in the previous mixed-valence literature. The classification by range of validity is of course somewhat arbitrary; particular cases can be clarified by reference to relevant figures in this paper. The range of validity of the model itself (and the desirability of extensions or refinements) can only become clear with systematic application to observed spectra.

Acknowledgments. This work was supported by the National Science Foundation under Grant CHE77-0311.

Appendix. Derivation of Equations 32 and 33

We start with two parabolic potential surfaces, $W_A(Q)$ and $W_J(Q)$, which have different curvatures, k_A and k_J, and whose minima are displaced horizontally by $2\Lambda/k_J$ and vertically by $(W_J^0 - W_A^0 - (2\Lambda^2/k_J))$. We assume that the electronic functions associated with the two surfaces are independent of Q so that simple Born-Oppenheimer vibronic functions, $|A\rangle|a\rangle$ and $|J\rangle|j\rangle$, are appropriate.

The Hamiltonian operator may be written

$$H = H_{el} + T_n \qquad \text{(A1)}$$

where T_n is the nuclear kinetic energy operator ($= P^2/2$) and Q is mass normalized. Then

$$H_{el}|A\rangle = W_A(Q)|A\rangle \qquad H_{el}|J\rangle = W_J(Q)|J\rangle \tag{A2}$$

with

$$W_A(Q) = W_A{}^0 + \tfrac{1}{2}k_AQ^2$$

$$W_J(Q) = W_J{}^0 + 2\Lambda Q + \tfrac{1}{2}k_JQ^2 \tag{A3}$$

and

$$\left(\tfrac{1}{2}k_AQ^2 + T_n\right)|a\rangle \equiv H_a|a\rangle = |a\rangle\left(n_a + \tfrac{1}{2}\right)h\nu_a$$

$$\left((2\Lambda Q + \tfrac{1}{2}k_JQ^2 + T_n)|j\rangle \equiv H_j|j\rangle = |j\rangle\left(n_j + \tfrac{1}{2}\right)h\nu_j \tag{A4}$$

Assuming a δ function line width with only the vibronic levels of electronic state $|A\rangle$ populated, substituting eq 23 into eq 21 yields[16]

$$\bar{E} = \sum_{a,j,j'} \frac{N_a}{N}\langle a|j\rangle\left(\langle Jj|H|Jj'\rangle - \langle Aa|H|Aa\rangle\,\delta_{jj'}\right)\langle j'|a\rangle$$

$$\langle\alpha\rangle_2{}^{\bar{E}} = M^2\sum_{\substack{a,j,\\ j',j''}} \frac{N_a}{N}\langle a|j\rangle\left(\langle Jj|H|Jj'\rangle - \langle Aa|H|Aa\rangle\delta_{jj'} - \bar{E}\delta_{jj'}\right)\left(\langle Jj'|H|Jj''\rangle - \langle Aa|H|Aa\rangle\delta_{j'j''} - \bar{E}\delta_{j'j''}\right)\langle j''|a\rangle \tag{A5}$$

In obtaining eq A5, the Franck-Condon approximation has been made (so M^2 is the absolute square of the *electronic* transition moment), and use has been made of the fact, following from eq A2-A4, that $\langle Jj|H|Jj'\rangle = \langle Jj|H|Jj\rangle\delta_{jj'}$ (so that $\langle Jj|H|Jj\rangle = \Sigma_{j'}\langle Jj|H|Jj'\rangle$). N_a is the concentration of molecules in ground vibronic state $|Aa\rangle$ and N is the total molecular concentration. Noting that $\Sigma_j|j\rangle\langle j| = \Sigma_a|a\rangle\langle a|$, the summations over excited-state vibrational functions can be replaced by summations over ground-state vibrational functions. Then using eq A2-A4, eq A5 become

$$\bar{E} = (W_J{}^0 - W_A{}^0) + \overline{\langle a|H_j - H_a|a\rangle}$$

$$\langle\alpha\rangle_2{}^{\bar{E}} = M^2\left[\overline{\langle a|H_j{}^2|a\rangle} - \left(\frac{k_J}{k_A}\right)\overline{\langle a|H_a|a\rangle^2} - \left(\overline{\langle a|H_a|a\rangle}\right)^2\left(\frac{k_J - k_A}{2k_A}\right)^2\right] \tag{A6}$$

where the bar over a symbol designates thermal average (e.g., $\overline{\langle a|H_j|a\rangle} \equiv \Sigma_a\,(N_a/N)\,\langle a|H_j|a\rangle$, etc.), and $4\pi^2\nu_a{}^2 = k_A$. Noting that[21] $\langle a|P^2|a\rangle = k_A\langle a|Q^2|a\rangle = \langle a|H_a|a\rangle$, $\langle a|Q^2P^2|a\rangle = \langle a|P^2Q^2|a\rangle = (h^2/16\pi^2)\,(2n_a{}^2 + 2n_a - 1)$, $\langle a|P^4|a\rangle = k_A{}^2\,\langle a|Q^4|a\rangle = (3/4)(h\nu_a)^2\,(2n_a{}^2 + 2n_a + 1)$, the required thermal averages are[22] $\langle a|H_a|a\rangle = (h\nu_a/2)\coth(\beta/2)$, $\overline{(2n_a{}^2 + 2n_a + 1)} = \coth^2(\beta/2)$ with $\beta \equiv h\nu_a/kT$, and eq A6 become

$$\bar{E} = (W_J{}^0 - W_A{}^0) + \left(\frac{1}{4}\right)h\nu_a\left(\frac{k_J - k_A}{k_A}\right)\coth(\beta/2)$$

$$\frac{\langle\alpha\rangle_2{}^{\bar{E}}}{M^2} = \frac{1}{8}(h\nu_a)^2\left(\frac{k_J - k_A}{k_A}\right)^2\coth^2(\beta/2) + (2\Lambda^2/k_A)h\nu_a\coth(\beta/2) \tag{A7}$$

If the minima in both potential surfaces are at $Q = 0$, then $\Lambda = 0$ and eq A7 is equivalent to eq 32 with $\nu_a = \nu_1$, $k_J = k_2$, $k_A = k_1$. To obtain eq 33, we must express eq A3 in the same units as eq 1. Noting the relation $q = 2\pi(\nu_-/h)^{1/2}\,Q$ (eq 20, ref 7, with $M = 1$), setting $k_J = k_A$, $\nu_a = \nu_-$, and comparing eq A3 and eq 1 (with $\epsilon = 0$), we find $2Wh\nu_- = (W_J{}^0 - W_A{}^0 - (2\Lambda^2/k_A))$ and $\Lambda^2/k_A = \lambda^2h\nu_-$. Using this latter relationship (and $k_J = k_A$, $\nu_a = \nu_-$) in eq A7 yields eq 33.

References and Notes

(1) (a) University of Virginia; (b) Randolph-Macon Woman's College.
(2) M. B. Robin and P. Day, *Adv. Inorg. Chem. Radiochem.*, **10**, 247 (1967).
(3) For recent work, see, for example, T. J. Meyer, *Acc. Chem. Res.*, **11**, 94 (1977), and references cited therein.
(4) (a) N. S. Hush, *Prog. Inorg. Chem.*, **8**, 391 (1967); (b) *Electrochim. Acta*, **13**, 1005 (1968).
(5) (a) J. J. Hopfield, *Biophys. J.*, **18**, 311 (1977), and references cited therein; (b) M. J. Potasek and J. J. Hopfield, *Proc. Natl. Acad. Sci. U.S.A.*, **74**, 229, 3817 (1977).
(6) J. K. Beattie, N. S. Hush, and P. R. Taylor, *Inorg. Chem.*, **15**, 992 (1976).
(7) S. B. Piepho, E. R. Krausz, and P. N. Schatz, *J. Am. Chem. Soc.*, **100**, 2996 (1978).
(8) P. N. Schatz, S. B. Piepho, and E. R. Krausz, *Chem. Phys. Lett.*, **55**, 539 (1978).
(9) To a first approximation, one need only consider a single coordinate, $q_- \equiv q = C'(Q_A - Q_B)$, to discuss the potential surfaces relevant to the spectroscopy of these systems.[7] C' is a constant and Q_A and Q_B are the a_{1g} normal coordinates of the two octahedral monomer units. ν_- is the vibrational frequency associated with q. For the Creutz and Taube complex, for example, $h\nu_- \approx 500$ cm^{-1}.
(10) R. Englman, "The Jahn-Teller Effect in Molecules and Crystals", Wiley-Interscience, New York, 1972, Sections 3.6 and 7.7.
(11) R. L. Fulton and M. Gouterman, *J. Chem. Phys.*, **35**, 1059 (1961); **41**, 2280 (1964).
(12) M. Lax, *J. Chem. Phys.*, **20**, 1752 (1952).
(13) Y. Toyozawa and M. Inoue, *J. Phys. Soc. Jpn.*, **21**, 1663 (1966).
(14) A. Messiah, "Quantum Mechanics", Vol. 1, North-Holland Publishing Co., Amsterdam, 1969, Appendix AII.
(15) Charles Kittel, "Introduction to Solid State Physics", 4th ed., Wiley, New York, 1971, p 703.
(16) Reference 7, eq A7. Note that the last parentheses in the last of these three equations should read $(E_\nu - E_{\nu'} - \bar{E})^2$; i.e., $\bar{E}$ was inadvertently omitted.
(17) R. Kubo and Y. Toyozawa, *Prog. Theor. Phys.*, **13**, 160 (1955).
(18) See, for example, S. R. Cooper and M. Calvin, *J. Am. Chem. Soc.*, **99**, 6623 (1977); M. J. Powers and T. J. Meyer, *Inorg. Chem.*, **17**, 1785 (1978).
(19) A. von Kameke, G. M. Tom, and H. Taube, *Inorg. Chem.*, **17**, 1790 (1978).
(20) B. Badger and B. Brocklehurst, *Trans. Faraday Soc.*, **85**, 2582, 2588 (1969).
(21) E. B. Wilson, Jr., J. C. Decius, and P. C. Cross, "Molecular Vibrations", McGraw-Hill, New York, 1955, Appendix III. (Note the correction: $(P^2)_{vv} = (h^2/4\pi^2)(v + \frac{1}{2})\gamma$.)
(22) M. Born and K. Huang, "Dynamical Theory of Crystal Lattices", Oxford University Press, London, 1954, Chapter IV, §16.
(23) L. Atkinson and P. Day, *J. Chem. Soc. A.*, 2423 (1969).